ResearchGate

See discussions, stats, and author profiles for this publication at: https://www.researchgate.net/publication/51750037

Layer-by-Layer Self-Assembly of Chitosan and Poly(γ-glutamic acid) into Polyelectrolyte Complexes

ARTICLE *in* BIOMACROMOLECULES · DECEMBER 2011

Impact Factor: 5.75 · DOI: 10.1021/bm2008235 · Source: PubMed

CITATIONS
34

READS
164

9 AUTHORS, INCLUDING:

Joana C Antunes
French National Centre for Scientific Research
9 PUBLICATIONS **89** CITATIONS
SEE PROFILE

Catarina Leite Pereira
University of Porto
8 PUBLICATIONS **56** CITATIONS
SEE PROFILE

Raquel M Gonçalves
University of Porto
31 PUBLICATIONS **402** CITATIONS
SEE PROFILE

Mário A Barbosa
University of Porto
240 PUBLICATIONS **4,393** CITATIONS
SEE PROFILE

All in-text references underlined in blue are linked to publications on ResearchGate, letting you access and read them immediately.

Available from: Mário A Barbosa
Retrieved on: 28 January 2016

Article

pubs.acs.org/Biomac

Layer-by-Layer Self-Assembly of Chitosan and Poly(γ-glutamic acid) into Polyelectrolyte Complexes

Joana C. Antunes,*[,†,‡] Catarina Leite Pereira,[†] Maria Molinos,[†] Frederico Ferreira-da-Silva,[∥] Mariagemiliana Dessì,[⊥] Antonio Gloria,[⊥] Luigi Ambrosio,[⊥] Raquel M. Gonçalves,[†] and Mário A. Barbosa[†,§,⊥]

[†]INEB - Instituto de Engenharia Biomédica, [‡]Faculdade de Engenharia, and [§]Instituto de Ciências Biomédicas Abel Salazar, Universidade do Porto, Porto, Portugal

[∥]IBMC - Instituto de Biologia Molecular e Celular, Porto, Portugal

[⊥]Institute of Composite and Biomedical Materials, National Research Council, P.le Tecchio 80, 80125 Naples, Italy

ABSTRACT: Chitosan (Ch) is a nontoxic and biocompatible polysaccharide extensively used in biomedical applications. Ch, as a polycation, can be combined with anionic polymers by layer-by-layer (LbL) self-assembly, giving rise to multilayered complexed architectures. These structures can be used in tissue engineering strategies, as drug delivery systems, or artificial matrices mimicking the extracellular microenvironment. In this work, Ch was combined with poly(γ-glutamic acid) (γ-PGA). γ-PGA is a polyanion, which was microbially produced, and is known for its low immunogenic reaction and low cytotoxicity. Multilayered ultrathin films were assembled by LbL, with a maximum of six layers. The interaction between both polymers was analyzed by: ellipsometry, quartz crystal microbalance with dissipation, Fourier transform infrared spectroscopy, atomic force microscopy, and zeta potential measurements. Ch/γ-PGA polyelectrolyte multilayers (PEMs) revealed no cytotoxicity according to ISO 10993-5. Overall, this study demonstrates that Ch can interact electrostatically with γ-PGA forming multilayered films. Furthermore, this study provides a comprehensive characterization of Ch/γ-PGA PEM structures, elucidating the contribution of each layer for the nanostructured films. These model surfaces can be useful substrates to study cell−biomaterial interactions in tissue regeneration.

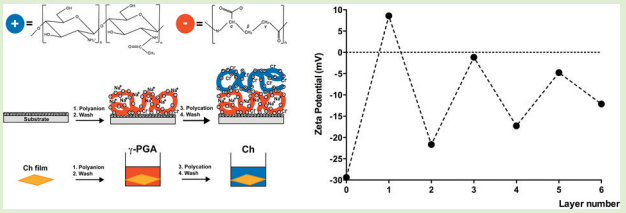

INTRODUCTION

The layer-by-layer (LbL) self-assembly technique involves polyelectrolyte multilayer (PEM) films preparation and is based on sequential adsorption of multiple thin polyion films from solutions with attractive interactions with each other.

The surface electrical charge reversal after each deposition step is a precondition for multilayer formation. Under commonly employed conditions, PEMs are dominated by electrostatic attractions, which are considered to be one of the driving forces for the LbL self-assembly.[1−3]

The concept of LbL self-assembly was first introduced by Iler[4] in 1966, describing the formation of multilayers by alternate deposition of positively and negatively charged colloid particles by adsorption from solution.[4,5] Decher et al. (1992) followed the pioneering work of Iler applying the concept to multilayered nanofilms,[6] and the LbL deposition technique became a mushrooming field of biomedical research.[7,8] In fact, the increasing interest in LbL self-assembled films is remarkable. Potential biomedical applications have been extensively described elsewhere.[1,7−9] PEM films have been studied for several applications, namely, as implantable device coatings, drug delivery systems, gene therapy, and tridimensional biomimetic cell/biomaterial constructs.[1,7−9] Examples of the latter include: Ch/heparin PEM film coatings on stainless-steel coronary stents in pigs;[10] glucose-sensitive hollow polyelectrolyte capsules, bearing phenylboronic acid moieties, for the controlled delivery of insulin;[11] cell-degradable polyethylenimine/short interfering RNA PEMs for sustained siRNA delivery targeting viral infection;[12] and cross-linked poly(L-lysine)/hyaluronan PEM films as reservoirs for rhBMP-2 delivery.[13] Additionally, the study of PEM films provides valuable tools for fundamental analyses to tune physical, chemical, and biochemical properties at the cell/material interface, as it has been also greatly described in the literature.[7]

The popularity of the versatile LbL methodology is based on: (i) its robustness and minimal setup, which turns it into a low cost method for multilayer fabrication;[1,14] (ii) the potential to modulate surface chemical, physical, and structural properties at the nanometer-level by changing, among others, the solution composition, pH, ionic strength, number of deposited layers, dipping and rinsing times, and film post-treatment;[15−17] and (iii) the possibility of introducing a large panoply of molecules into the multilayer in a programmed sequence, adding new functionalities.[14] Together, these features make this technique suitable for application in different substrates and for industrial production.[1]

Received: June 16, 2011
Revised: October 7, 2011
Published: October 28, 2011

ACS Publications © 2011 American Chemical Society

LbL self-assembly is a kinetically controlled method, and thus the control of the processing parameters is essential. The main factors influencing multilayer buildup are the pH, ionic strength, exposure time, polyion concentration, solvent quality, charge density of the polyions, type of polyelectrolyte, temperature, atmospheric humidity, rinsing step, and intermediate drying.[1,2,18]

The effect of pH on LbL self-assembly is particularly important in weak (only partially charged at pH near their pK_a) polyelectrolyte interactions.[1,7] The local pH values may differ from the external pH, thus controlling the distribution of the polyions in the layers.[2] Therefore, deducing the optimal pH range for interaction is an important step for the optimization of the processing parameters.

Chitosan (Ch) is a linear β-1,4-linked cationic polysaccharide derived from partial deacetylation of chitin, which consists of glucosamine and *N*-acetylglucosamine units.[19,20] The main parameters influencing its characteristics are molecular weight (M_w) and degree of acetylation (DA, representing the proportion of acetylated units).[21] This natural polymer is endowed with biochemical activity, biocompatibility, and enzymatic degradation into nontoxic products in vivo, properties that turn it into a very appealing material for biomedical applications.[19,21,22]

The primary amine groups of Ch can be exploited for the LbL self-assembly (Figure 1).[20] In acidic pH, these amines are

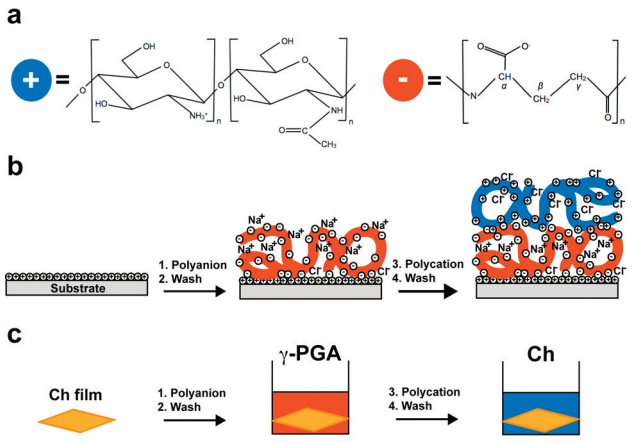

Figure 1. (a) Molecular units of both polymers used in the multilayer buildup: Chitosan (Ch, left), as a polycation, and poly(γ-glutamic acid) (γ-PGA, right), as a polyanion. (b) Simplified molecular picture of the first two deposition steps, illustrating film deposition starting with a positively charged surface. Counterions are included. Polyion conformation and layer intermingling are omitted for clarity. (c) Schematics of the layer-by-layer (LbL) deposition process, by horizontal immersion, using gold-coated silicon wafers as substrates, coated with a Ch film, obtained by spin-coating. Steps 1 and 3 represent the adsorption of the γ-PGA and Ch, respectively. Steps 2 and 4 are the intermediate rinsing with buffer solution. With such cyclic depositions, the simplest multilayer film architecture can be obtained (adapted from refs 6, 16, and 64).

positively charged, turning Ch into a water-soluble cationic polyelectrolyte. Ch's pK_a is near neutrality, close to 6.5, with the soluble–insoluble transition occurring at a pH between 6.46 and 7.32, depending on DA and M_w, which is a particularly convenient range for biological applications.[20,23,24]

As a polycation, Ch spontaneously forms polyelectrolyte complexes (PECs) with anionic polyelectrolytes, which has been explored with (i) natural polyanions, such as alginate, hyaluronic acid (HA), carrageenan, heparin, carboxymethyl cellulose, chondroitin sulfate, poly(glutamic acid) (PGA), dextran sulfate, and pectin, (ii) proteins like collagen and mucins, (iii) synthetic polyanions, such as poly(acrylic acid) and polyvinyl sulfate, or even (iv) DNA molecules.[21,25]

In particular, PGA is a biocompatible polymer that can be synthesized chemically (α-PGA) or produced microbially (γ-PGA), with use in several applications. This water-soluble poly(amino acid) is additionally a nontoxic and biodegradable biomaterial.[26] The naturally occurring γ-PGA is particularly advantageous for biomedical applications.[26,27] γ-PGA is an anionic polyelectrolyte with an isoelectric point of 2.19, due to a high content of carboxyl groups (Figure 1).[28] The existence of γ-PGA in mammals has been reported, suggesting that this polymer could be biochemically degraded into glutamic acid residues in vivo, whereas α-PGA cannot.[26,29] γ-PGA, first described as a constituent of the *Bacillus anthracis* surface capsule, does not elicit an immune response from the host.[30−32] The lack of immune response of γ-PGA was also demonstrated after injection in rats.[33−35]

Ch and PGA (mostly γ-PGA) PECs have previously been reported in literature in the form of multilayered films.[36,37] In these studies, a single characterization method – quartz crystal microbalance (QCM) – was used to detect the efficiency of PEM formation, and a significant amount of organic solvents was employed to improve film deposition and obtain a stable multilayer buildup. No confirmation of the chemical composition of the built films or of an electrostatic interaction was reported. Recently, Ch/γ-PGA PEC hydrogels,[38−40] nanoparticles,[41,42] and multilayered hollow nanocapsules[43] have also been studied. However, a study on how these complexes are molecularly assembled and how both polymers contribute to buildup a multilayer structure has never been carried out.

This work aims to combine Ch with microbially produced γ-PGA to produce PEM films, envisioning its use as model surfaces to investigate cell–biomaterial interactions in tissue regeneration.

MATERIALS AND METHODS

Chitosan Purification. Ch (France-Chitine) purification protocol was adapted from Crompton et al.[44] In brief, Ch was purified by dissolution in 0.1 M HCl and precipitation with dropwise addition of 0.1 M KOH. The precipitate was collected and rinsed with distilled deionized water until neutralization of the solution pH. The Ch obtained was freeze-dried for 48 h and milled into a fine powder. Purified Ch was stored protected from light and humidity until use.

Ch was characterized concerning the DA, the M_w, and the rheological behavior. The DA was determined by Fourier transform infrared spectroscopy (FTIR) spectrum. The Ch spectrum was determined with KBr pellets, and for the determination of the DA the amide III band (1320 cm^{-1}) and the analytical band (1420 cm^{-1}), as internal reference, were used, according to Brugnerotto et al.[45] The M_w was determined by size-exclusion chromatography. The weight-average molecular weight (M_w), the number-average molecular weight (M_n), and the polydispersion index (PDI) were determined with the 0.2 M CH_3COONa/0.5 M CH_3COOH/0.01% NaN_3 system as the mobile phase at room temperature, according to Terbojevich et al.[46] Table 1 summarizes the properties of the Ch used.

γ-PGA Production and Purification. γ-PGA was produced by *Bacillus subtilis* IFO3335.[47] The isolation method was adapted from the one described by Kubota et al.[48] and Ashiuchi et al.[49] γ-PGA molecular weight and purity grade were determined by SDS-PAGE,[50]

Table 1. Characterization of Ch and γ-PGA Used in the PEMs Preparation[a]

	DA (%)	$M_w \times 10^3$	$M_n \times 10^3$	PdI	viscoelastic properties	G' (mPa)	G'' (mPa)
Ch	10.4 ± 1.6	324 ± 27	151 ± 13	2.2 ± 0.3	5 mg/mL solution	0.56−41	65−640
					0.2 mg/mL solution	0.25−13	2.3−21
	$M_w \times 10^3$	D/L ratio	purity (%)	yield (mg/mL)	viscoelastic properties	G' (mPa)	G'' (mPa)
γ-PGA	10−50	50−60/40−50	∼99.5	0.2	0.2 mg/mL solution	0.12−6.7	0.75−14

[a]Characterization was performed after polymers purification, regarding the degree of acetylation (DA), molecular weight (M_w and M_n), polydispersion index (PdI), stereochemical composition (D/L ratio), purity grade, and yield of production. Ch (5 and 0.2 mg/mL) and γ-PGA (0.2 mg/mL) solutions were characterized regarding their viscoelastic properties at 25°C: shear storage modulus, $G'(\omega)$ and shear loss modulus, $G''(\omega)$ were evaluated within a 0.1 to 1 Hz frequency range.

and its stereochemical composition was evaluated by circular dichroism.[51] Table 1 summarizes the properties of the γ-PGA used.

Preparation of the Polyelectrolyte Complexed Films. *Substrates.* Gold-coated silicon wafers were prepared by Instituto de Engenharia de Sistemas e Computadores (INESC), as previously described,[52] and used as substrates for the multilayer buildup. In brief, gold substrates were prepared using an automated, load-locked ion beam deposition system (Nordiko N3000). Details of the machine can be found elsewhere.[53] Chromium (5 nm) and gold (25 nm) films were deposited by ion beam sputtering from gold and chromium targets (99.9% purity) onto silicon wafers (polished/etched, crystal orientation 100, from Aurel Gmbh). The thin layer of chromium was used to improve adhesion of gold to silicon. Deposition rates were 0.050 nm/s for chromium and 0.033 nm/s for gold. Deposition pressure was 3.5×10^{-5} Torr. The wafers were diced into pieces (1×1 cm^2) using a DISCO DAD 321 automated saw. Before dicing, all wafers were coated with 1.5 μm of photoresist (PFR7790EG, JSR Electronics), which is soluble in acetone, to protect the film surface.

Gold substrates were cleaned twice in acetone and immersed in "piranha" solution (7:3 volume ratio of concentrated H_2SO_4 and H_2O_2) for 5 min. (*Caution: This solution reacts violently with many organic materials and should be handled with extra care.*) Substrates were rinsed sequentially with ethanol, ultrapure water, and ethanol in an ultrasonic bath.

In in vitro cell culture studies, borosilicate cover glass discs of 13 mm of diameter (VWR) were used for the multilayer buildup. Before use, the borosilicate cover glass discs were immersed in 65% HNO_3 overnight. The glass discs were then extensively washed with ultrapure water and dried separately at 220 °C overnight.

Ch Ultrathin Films. Ch ultrathin films were prepared by spin-coating. In brief, Ch (5 mg/mL in 0.2 M CH_3COOH) was spin-coated onto clean gold/glass substrates, during 120 s, at 9000 rpm, neutralized with NaOH (Merck) 0.1 M (5 min), rinsed two times in ultrapure water, and dried with an argon stream and then in an oven at 37 °C for 24 h.

Layer-by-Layer Deposition. Ch/γ-PGA PEM films were prepared by alternate immersion in Ch and γ-PGA solutions at pH 5. First, the gold/glass substrates carrying the Ch ultrathin films were immersed into a γ-PGA solution (0.2 mg/mL, in buffer: 0.05 M Tris-HCl, 0.15 M NaCl (Sigma)) during 15 min. Afterward, the substrates were immersed in a Ch solution (0.2 mg/mL, in 0.2 M CH_3COOH (Panreac)), and the process was repeated until six layers were deposited. Between each layer, the samples were washed in buffer solution for 2 min. All deposition steps were performed under a gentle orbital shaking (100 rpm). After film deposition, the surface was rinsed twice with ultrapure water and dried for 24 h at 37 °C. The films were then maintained in an argon-filled container until further characterization (maximum: 24 h).

Viscoelastic Properties of the Polymeric Solutions. The viscoelastic properties of both polymer solutions were studied at Institute of Composite and Biomedical Materials, National Research Council, Naples, Italy. Small amplitude oscillatory shear tests were performed at 25 °C on Ch and γ-PGA solutions (5 and 0.2 mg/mL Ch in 0.2 M CH_3COOH and 0.2 mg/mL γ-PGA in 0.05 M Tris-HCl with 0.15 M NaCl buffer). A rotational rheometer (Gemini, Bohlin, Sweden) was used with a double gap configuration, the oscillation frequency ranging from 0.1 to 1 Hz, and a strain amplitude at which linear viscosity is attained.[54] A solvent trap was also used to prevent water evaporation during measurements. The dynamic moduli G' (storage modulus or elastic modulus) and G'' (loss modulus or viscous modulus) were evaluated in the frequency range investigated. Table 1 summarizes the data obtained.

Characterization of the Polyelectrolyte Multilayer Films. *Imaging Ellipsometry.* The PEMs thickness was estimated by imaging ellipsometry. The ellipsometer (model EP3, from Nanofilm Surface Analysis) was operated in a polarizer-compensator-sample-analyzer (PCSA) mode (null ellipsometry). The light source was a solid-state laser with a wavelength of 532 nm. Refractive index (n) and extinction coefficient (k) of the gold substrate were determined by using a delta and psi spectrum with a variation of angle between 67 and 72°. To determine the PEMs thickness, the same kind of spectrum was used, and n and k of the Ch layer were set at 1.54 and 0, respectively. A representative experiment was considered, with average of 18 regions of interest (ROIs) of two equivalent samples of each condition.

Atomic Force Microscope (AFM). The PEMs surface topography and roughness were assessed by AFM. AFM measurements were performed using a PicoPlus scanning probe microscope interface with a PicoScan controller from Agilent Technologies, Santa Clara, CA, USA. The instrument was operated with a 10×10 μm^2 piezoscanner, in tapping mode, with a scan speed set to 0.6 lines/second. The imaging and surface roughness analysis were performed from scanned areas of 5×5 μm^2 on three randomly chosen locations of each sample, in air and in liquid, at room temperature. In liquid conditions, the samples were analyzed with filtered ultrapure water (0.2 μm pore size filter). The pH of water was adjusted to 5 for PEM films. The root-mean-square (rms) roughness within the sampling area was determined using the WSxM scanning probe microscopy software,[55] according to

$$\mathrm{RMS} = \sqrt{\frac{\sum_{i,j}(a_{i,j} - \langle a \rangle)^2}{N}} \quad (1)$$

where a are the image heights and N is the total number of points.

In air, a bar-shaped silicon cantilever (ACT probe, from AppNano), with a spring constant of 25−75 N/m, was used for the gold-coated silicon wafers. For the Ch and PEM films, a bar-shaped silicon cantilever (FORT probe, from AppNano) was selected, with a spring constant of 1−5 N/m.

Under liquid conditions, for the gold substrates, the bar-shaped silicon cantilever (FORT probe, from AppNano) with a spring constant of 1−5 N/m was selected. For PEM films, a gold-coated v-shaped silicon nitride cantilever with a spring constant of 0.12 N/m (NP probe, from Scientec) was used.

Fourier Transform Infrared Spectroscopy. Fourier transform infrared reflection absorption spectroscopy (FTIR-IRRAS) measurements were performed to evaluate the surface chemical composition of the complexes formed after LbL assembly. An FTIR spectropho-

tometer from Perkin-Elmer (model 2000) coupled to VeeMax II Accessory (PIKE) and a liquid-nitrogen cooled MCT detector were used. The instrument was continuously purged with dry nitrogen for 3 min before data collection and during measurements to eliminate water vapor absorption. Spectra were collected using the 80° grazing angle reflection mode. The incident light was p-polarized, and a gold surface was used as the background. The γ-PGA spectrum was obtained with KBr pellets. For each sample, 200 scans were collected with 4 cm^{-1} resolution.

Electrokinetic Analyzer. The ζ potential after each PEM layer deposition was determined from streaming potential measurements with a commercial electrokinetic analyzer (EKA) (Anton Paar GmbH, Austria) using the so-called "Stamp Cell", designed for small rectangular samples, as described elsewhere.[56,57] The Stamp Cell is composed of two poly(methyl methacrylate) (PMMA) sample holders with a cross-section of 1 × 2 cm^2, which accommodate a pair of rectangular samples of the same size. A defined gap between the sample surfaces is achieved by means of a micrometer screw. The electrolyte is circulated through this gap, thereby creating a differential pressure to shear off the diffuse part of the electrochemical double layer at the sample/electrolyte interface. The streaming potential was measured by Ag/AgCl electrodes, which are installed at both ends of the streaming channel. The specimen is fixed on the respective PMMA piston with a double-sided adhesive tape for measurement. The gap between the planar samples was adjusted by using the scale of a micrometer screw and by monitoring the electrolyte flow in the measuring cell. Two samples (1 × 1 cm^2) were glued on each PMMA sample holder and mounted in the Stamp Cell. The electrolyte used was KCl (VWR), 1 mM and pH 5, and experiments were performed at room temperature. The conductivity of the electrolyte solution was measured during the experiments. The streaming potential was measured while applying an electrolyte flow with alternative direction and pressure ramps from 0 to 400 mbar. For each measurement, eight pressure ramps were performed (four in each flow direction).

The ζ potential was calculated according to the Fairbrother–Mastin[58] method, which is included in the software package (VisioLab) accompanying the equipment.

Quartz Crystal Microbalance with Dissipation (QCM-D). The multilayer buildup of PEMs was followed in real time using the dissipation enhanced QCM-D E4 system from Q-Sense AB. The QCM-D crystals were AT-cut quartz crystals (Q-Sense AB). The diameter of the crystals was 14 mm, the fundamental frequency (f_0) was 4.95 MHz, and the sensitivity constant (C) was 0.177 mg/m^2 Hz. Prior to use, the quartz crystals were cleaned in the following way: exposure to UV/ozone for 10 min to remove hydrocarbons and organic contaminants and render the surfaces hydrophilic; this was followed by immersion into a 1:1:5 solution by volume of H_2O_2 (30%), NH_4OH (25%), and ultrapure water for 5 min at 75 °C. Subsequently, the quartz crystals were thoroughly rinsed with ultrapure water and dried with argon, being then assembled into the QCM-D chamber ready to use.

The LbL self-assembly on the surface of gold-coated quartz crystal, previously coated with a thin film of Ch by spin-coating, was achieved by flowing γ-PGA and Ch solutions (0.2 mg/mL) in an alternating manner $(\gamma\text{-PGA/Ch})_5$ through the QCM-D flow cell (0.42 mL/min), with intermediate washing with the 0.05 M Tris-HCl with 0.15 M NaCl buffer solution. The deposition time for each layer was 15 min; the rinsing time with the buffer solution was 2 min. The temperature in the measurement chamber was stabilized at 25 ± 0.05 °C. The experiment was performed in triplicate and normalized to the fundamental resonant frequency of the quartz crystal (4.95 MHz). Data were modeled using the software Q-Tools provided by Q-Sense, according to the Voigt model.[59] All solution densities were measured using 10 mL glass picnometers in triplicate (1008 ± 2 kg/m^3). For the adsorbed layer, an estimated density of 1200 kg/m^3 was used.

In Vitro Cytotoxicity Assessment. Before cell culture, the PEMs were sterilized immediately before use by immersion in ethanol 70% during 1 h and rinsed three times with phosphate-buffered saline (PBS). NIH3T3 mouse embryonic fibroblast cell line was used to evaluate the cytotoxicity of 2D PEMs according to ISO 10993-5. In direct contact cultures, PEMs were then preincubated with RPMI 1640 liquid cell culture medium (1×, Invitrogen) + 10% fetal bovine serum (FBS, VWR) + 1% penicillin-streptomycin (Invitrogen) 30 min before cell seeding. NIH3T3 cells (12 500 cells/cm^2) were cultured in the cell culture medium described above, in direct contact with Ch/γ-PGA PEMs, in the presence of PEMs extracts and in tissue-culture treated polystyrene (TCPS) as a control. The materials extracts were prepared by incubation of the Ch and PEM films with RPMI 1640 culture medium, at 37 °C, with strong agitation (150 rpm), during 72 h. The culture medium obtained was filtered (0.2 μm pore size filter) and supplemented with 10% FBS, after which it was used to culture NIH3T3 cells. Cytotoxicity was evaluated by checking the metabolic activity through the Rezasurin test during 72 h each day. Three independent experiments (with three replicates each) were performed. The results presented refer to one representative experiment. Phase-contrast images, acquired using an inverted microscope (Axiovert, Zeiss), were taken to NIH3T3 cells in direct contact with all samples, 6 and 48 h after cell seeding.

Statistical Analysis. Results are presented as the mean plus/minus the standard deviation (SD). Statistical analysis was performed using GraphPad Prism version 5.0a. D'Agostino and Pearson omnibus normality test was used to assess Gaussian distribution of data. Parametric one-way ANOVA test was used to compared the groups of data from ellipsometry, with the Tukey's multiple comparison test as confirmation test. The nonparametric Mann–Whitney test was used to compare the groups of data of cytotoxicity studies. In both cases, a confidence level of at least 95% ($p < 0.05$) was considered.

RESULTS

Ch/γ-PGA Multilayer Films Characterization. The study of complexed Ch/γ-PGA PEM films requires characterization on the nanoscale. For that, PEM films were characterized regarding thickness, surface topography and roughness, surface chemical composition, surface electrical charge, and viscoelastic properties after each layer addition. Finally, the cytotoxicity of the films was analyzed. Ch/γ-PGA PEMs with a maximum of six layers were produced because with this number a complex system with a simple interlayer architecture was obtained, thus facilitating the analysis of the interactions on the nanometer-level.

Film Thickness. Through imaging ellipsometry, the film thickness in a dried state was determined as a function of the layer number (Figure 2). The results obtained indicate a regular

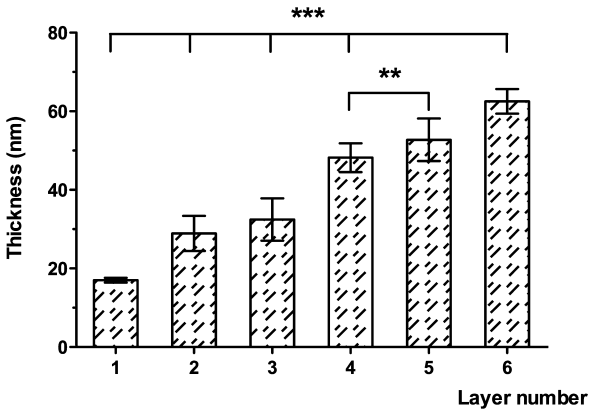

Figure 2. Ellipsometric film thickness of PEM films for each of the six layers. Odd layers are from Ch; even from γ-PGA. Results are present as mean ± StDev of 18 regions of interest (ROIs) ($n = 2$) from a representative experiment and are significantly different between different layers ($0.001 < **p < 0.01$ and $***p < 0.001$).

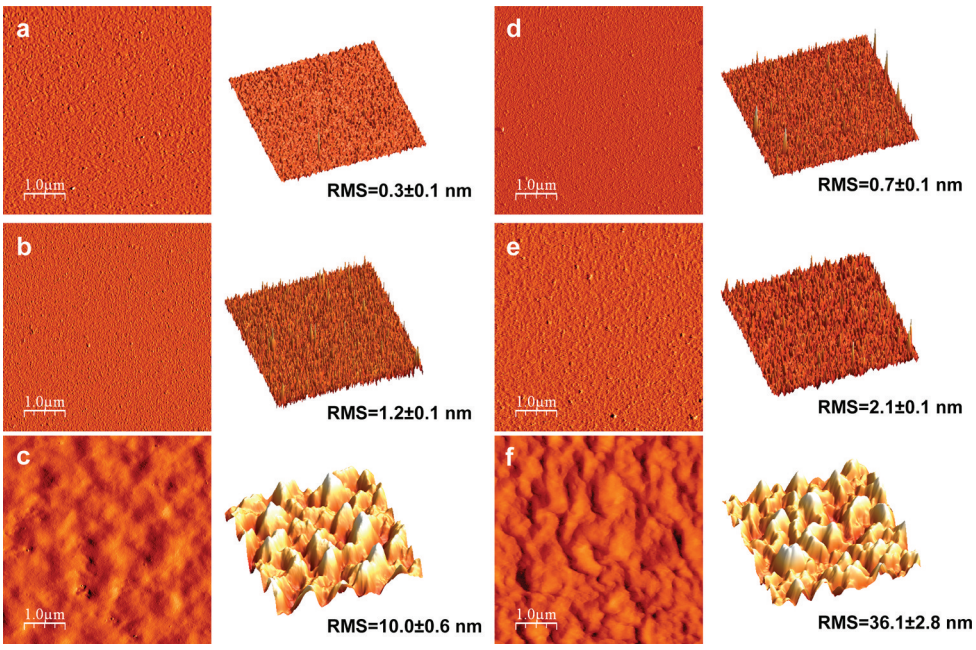

Figure 3. AFM amplitude (left) and 3D height (right) images obtained in a dried state of (a) gold substrate, (b) Ch film, and (c) $(Ch/\gamma\text{-PGA})_3$ PEM film, and under liquid conditions of (d) gold substrate, (e) Ch film, and (f) $(Ch/\gamma\text{-PGA})_3$ PEM film. The root-mean-square (rms) roughness is represented as mean ± SD of three independent areas of two replicates of each type of surface.

and significant ($p < 0.05$) increase in film thickness with each polyelectrolyte deposition. The PEM thickness increments started from a 17.0 ± 0.6 nm layer of a homogeneously distributed Ch film deposited by spin-coating. This provided the basic substrate for the alternating γ-PGA and Ch layers. With immersion in the first polyelectrolyte anionic solution (γ-PGA), the thickness increased until 29 ± 4 nm. Upon immersion in a Ch solution, it increased to 32 ± 5 nm. The final dried thickness, after the fifth polyelectrolyte immersion, was 63 ± 3 nm.

Atomic Force Microscopy. The surface topography of Ch films and Ch/γ-PGA PEMs were very distinctive when observed under AFM, as it can be seen in Figure 3. In a dried state (Figure 3a–c), the Ch coating was homogeneously distributed throughout the substrate (gold) surface, and its deposition did not cause a significant increase in the rms roughness (from 0.3 ± 0.1 to 1.2 ± 0.1 nm). After the LbL deposition, the topography underwent appreciable changes. Large structures, with some square micrometers of surface area, were displayed at this point of the materials processing. Accordingly, the superficial roughness increased considerably, to 10.0 ± 0.6 nm, over a scanned area of 25 μm^2. In liquid conditions, the surface topography was maintained in all samples. Comparing the wet and dry states, the surface roughness increased for the Ch films (Figure 3e) and even more significantly for the PEM films (Figure 3f). The rms roughness of the Ch and PEM films increased to 2.1 ± 0.1 and 36.1 ± 2.8 nm, respectively.

Surface Chemical Composition. The films'surface chemical composition was analyzed by FTIR. The spectra of the Ch/γ-PGA complexed films were compared with the spectra of both polymers alone (Figure 4a,b). The characteristic saccharide peaks of Ch in the 960–1180 cm^{-1} region can be observed: the C–O stretching absorption band at 1077 and 1034 cm^{-1} and the C–O–C asymmetric stretching vibrations at ~1145 cm^{-1}. A broad brand in the later region can also be observed in the γ-PGA spectrum, which relates to polysaccharides inclusion in the γ-PGA powder (Figure 4b). Other vibrations consist of the C═O stretching vibrations of secondary amides in the solid form and of saturated aliphatic carboxylic acid dimers like γ-PGA (amide I band, adsorption at 1630–1680 cm^{-1}), the N–H scissoring deformation peak at 1565 cm^{-1}, indicative of the presence of saturated primary amine groups, and also the N–H deformation and C–N stretching of secondary amides solids, which include the amide II band of γ-PGA. The two latter bands appear to be overlapped because of to the low energy associated with the spectra acquisition of the nanofilms and because of the bands proximity. The 1470–1590 cm^{-1} region results from both the N–H bending and the C–N stretching vibrations of the –CO–NH– group in its trans form, with a main contribution of the N–H bending motion.

With the LbL buildup, a new peak arises at 1220 cm^{-1}, suggesting the presence of γ-PGA (Figure 4). This peak is indicative of the C–O stretching of carboxylic acid dimers (which adsorb in the 1320–1210 cm^{-1} region), present in γ-PGA spectrum (Figure 4b), and may have also a contribution of the in-phase combination of N–H in-plane bending and C–N stretching vibrations of secondary amides (trans form), present in both polymers (incorporating the amide III of γ-PGA). Corroborating this observation, the C═O stretching band appears with an increased intensity with layer number, between 1595 and 1716 cm^{-1}. The same effect is observed with the N–H bending band, which is present in the 1482–1595 cm^{-1} region. With polyelectrolyte depositions (layers 2 to 6), the broad band of the saccharide peak area increases. A highest peak at 1100 cm^{-1} can be observed in Figure 4a. This increment is mainly due to Ch deposition, but is also present in the γ-PGA (Figure 4b). Finally, a shift in the position of the peak, in the 1595–1716 cm^{-1} region, to a lower wavenumber can be followed after contact of the initial Ch film with the polyions solutions (Figure 4a). All together, these observations

dx.doi.org/10.1021/bm2008235|*Biomacromolecules* 2011, 12, 4183–4195

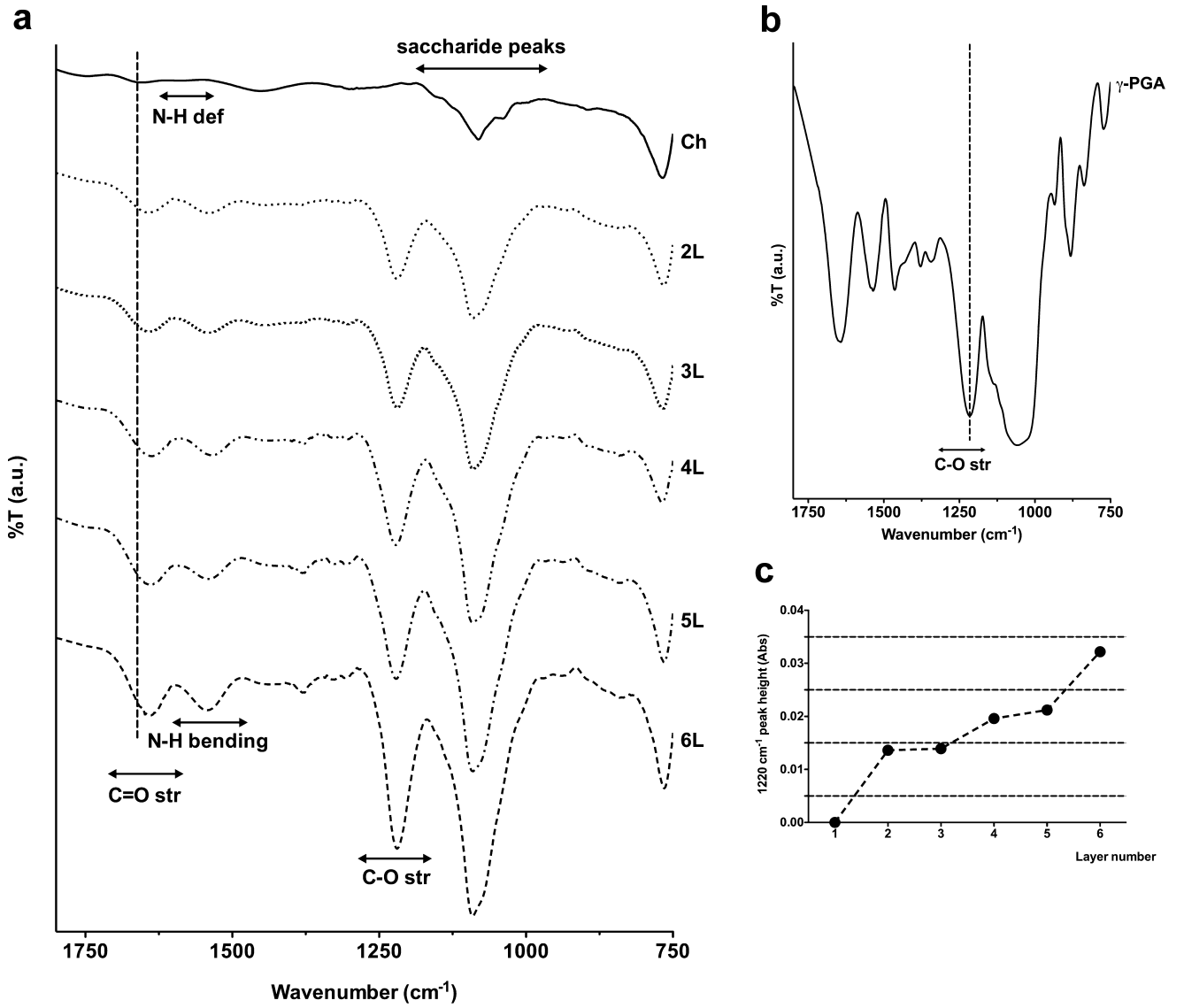

Figure 4. FTIR spectra of Ch, γ-PGA and PEM films. (a) FTIR-IRRAS spectra of Ch and Ch/γ-PGA PEM films, after each layer deposition, and major peak assignments, (b) FTIR-KBr spectrum of γ-PGA powder, and (c) peak height of the FTIR-IRRAS PEM spectra peak at 1220 cm^{-1} as a function of layer number.

suggest the presence of γ-PGA in the complexes and its electrostatic interaction with Ch.

ζ Potential Measurements. The streaming potential method was employed to determine the ζ potential of the films after deposition of each polyelectrolyte layer. Figure 5 represents the oscillation of the ζ potential of the substrate after each layer deposition, which is indicative of adsorption of consecutive layers of opposite electrical charge.

The gold substrate (layer number = 0) was negatively charged (−29.4 ± 0.5 mV). With the addition of the first Ch layer, a cationic polymer, the surface became positively charged (8.6 ± 0.8 mV). Upon deposition of the γ-PGA layer, the ζ potential was rendered negative (−22 ± 4 mV). With the second Ch layer, it increased again (−1 ± 1 mV). The same trend was followed until layer 6 was deposited. Upon deposition of each layer, a ζ potential inversion occurred. Furthermore, a decrease in the amplitude of the ζ potential inversion was detected.

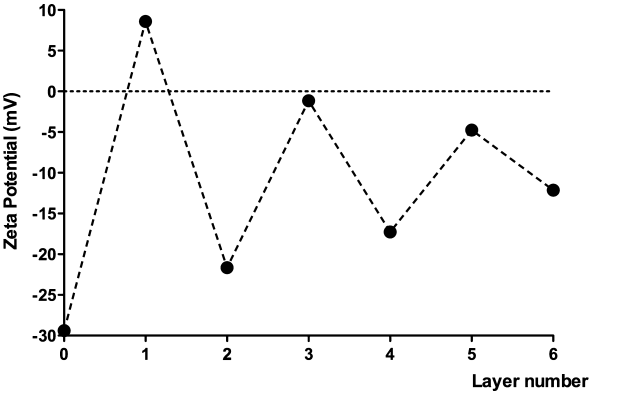

Figure 5. Evolution of the ζ potential (millivolts) with the alternate deposition of Ch and γ-PGA as a function of the layer number (one representative experiment, from four replicates).

QCM-D Viscoelastic Modeling. To confirm the multilayer buildup in real time, we used QCM-D. A gold-coated quartz crystal covered with a Ch film, previously deposited by spin-coating, was mounted in the chamber. Subsequently,

dx.doi.org/10.1021/bm2008235|Biomacromolecules 2011, 12, 4183–4195

alternating layers of γ-PGA and Ch were deposited, as described above. Figure 6a,b shows the frequency and

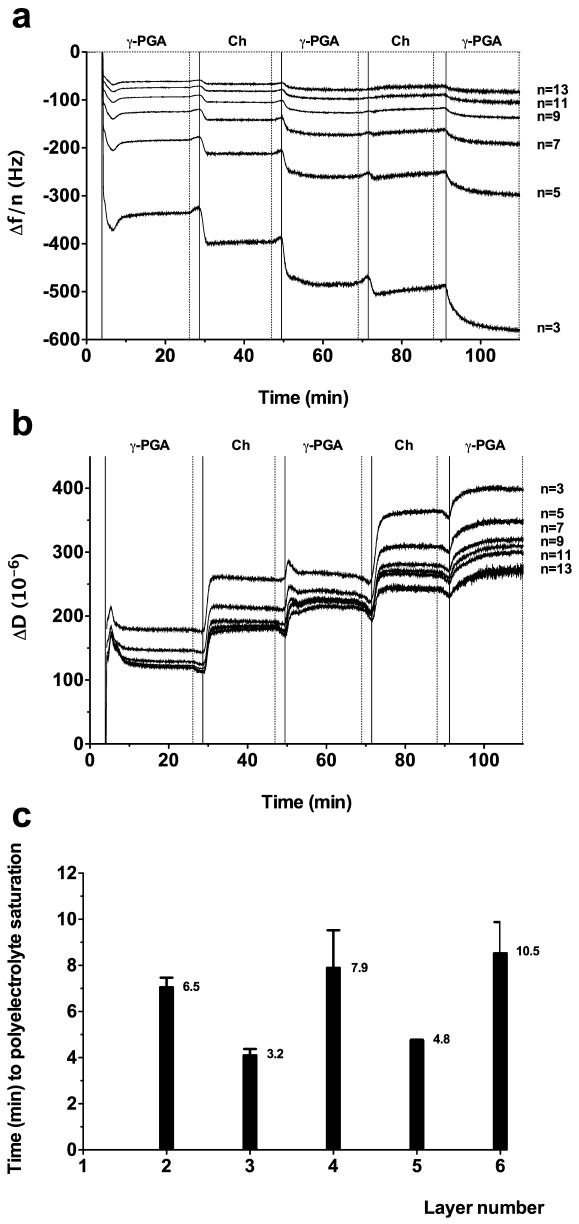

Figure 6. Differences in QCM-D frequency, dissipation, and time to saturation as polyelectrolyte layers are deposited on the quartz crystals, previously coated with a Ch film, by spin-coating. (a) Normalized change in frequency ($\Delta f/n$) and (b) dissipation (ΔD) as a function of adsorption time for the overtones n = 3, 5, 7, 9, 11, and 13. In both plots, the vertical continuous lines mark the polyelectrolyte addition and the dashed lines mark the washing with the buffer solution. (c) Time to polyelectrolyte saturation, at each layer deposition, obtained from the Voigt-modeled thickness values as a function of adsorption time (estimated for overtones n = 3, 5, 7, 9, 11 and 13; ρFld = 1008 kg/m^3; ηFld = 0.001 Pa·s; ρL1 = 1200 kg/m^3). Raw data from two independent experiments.

dissipation shifts associated with each polymer layer, as a function of adsorption time. The frequency change was normalized by the respective overtone number, as suggested by Hook et al.[60]

In Figure 6c, it is possible to observe that the adsorption of each polyion reaches saturation after a period that ranges from 3 to 11 min. Interestingly, the time to polyelectrolyte saturation was lower for Ch (3.2−4.8 min) than for γ-PGA layers (6.5−10.6 min). The sequential and alternate addition of γ-PGA and Ch solution resulted in a decrease in frequency, which was more intense for the γ-PGA additions (Figure 6a). When the buffer solutions were flushed though the cells, this resulted in a slight desorption of loosely adsorbed polyions, with a consequential increase in the frequency oscillation of the quartz crystals.

Using the software QTools, from Q-Sense, the Voigt model[59] was fitted to the data, to estimate time to polyelectrolyte saturation and film thickness (Figures 6c and 7d, respectively).

In Figure 7a, the highest frequency shifts were observed upon γ-PGA addition to the flow system. Figure 7b shows that Ch depositions had a major influence on the dissipation energy increments. Therefore, in Figure 7c, the ratio $\Delta D/(\Delta f/n)$, which measures the dissipation energy per unit frequency shift,[60−62] showed a higher increase after the Ch layers deposition. An exception to this behavior was found for the first γ-PGA addition.

Figure 7d represents the film thickness obtained by applying the Voigt model, together with the ellipsometric thickness of the Ch spin-coated film (layer number 1 in the Figure). The results depict a monotonic thickness increment with the LbL deposition.

The Sauerbrey model is frequently used in the literature in the study of rigid, evenly distributed, and sufficiently thin adsorbed layers.[60,63] Because high dissipation values were observed in our experiments (Figure 6b) and a distinct frequency (overtone)-dependence response was found, the Voigt[59] model is the most adequate in this situation. This model is valid for viscoelastic layers composed of macromolecules and water molecules trapped within the film.[60]

To obtain a complete interpretation of the process of multilayer buildup, the results obtained by different techniques (ellipsometry, FTIR, EKA and QCM-D) were normalized and compared for each layer (Table 2). The thickness increments (ellipsometry and QCM-D data) were determined regarding the contribution of each layer to the final thickness. With the FTIR, the C−O stretching peak increment was considered after the first γ-PGA deposition. Through the EKA analyses, the ζ potential difference, resulting from each layer addition to the substrate, was quantified.

After placing these results together, other important aspects became clearer: (i) In the ellipsometry results, higher thickness increments were observed with γ-PGA deposited layers. This may be due to a higher amount of γ-PGA being adsorbed in each deposition step or conformational changes that contribute to an increased thickness. (ii) In QCM-D, higher thickness increments, as calculated by the Voigt model, are observed for layers 3 and 5 (Ch depositions). This result is consistent with the rheological measurements performed with the polyelectrolyte solutions (Table 1) because the Ch solution has shear loss modulus (G'') values greater than the γ-PGA solution (and consequently a higher shear viscosity of the polyelectrolyte solution). Upon γ-PGA addition, the thickness increment was lower. For the same reason, (iii) when analyzing the FTIR-IRRAS peak at 1220 cm^{-1}, its magnitude is enhanced when γ-PGA is added to the multilayer, indicating that the major cause for the appearance of this peak appearance is the polyanion inclusion in the film. The same peak suffers a smaller increment upon Ch adsorption. This fact can be related to the contribution of the in-phase combination of N−H in-plane

dx.doi.org/10.1021/bm2008235|Biomacromolecules 2011, 12, 4183−4195

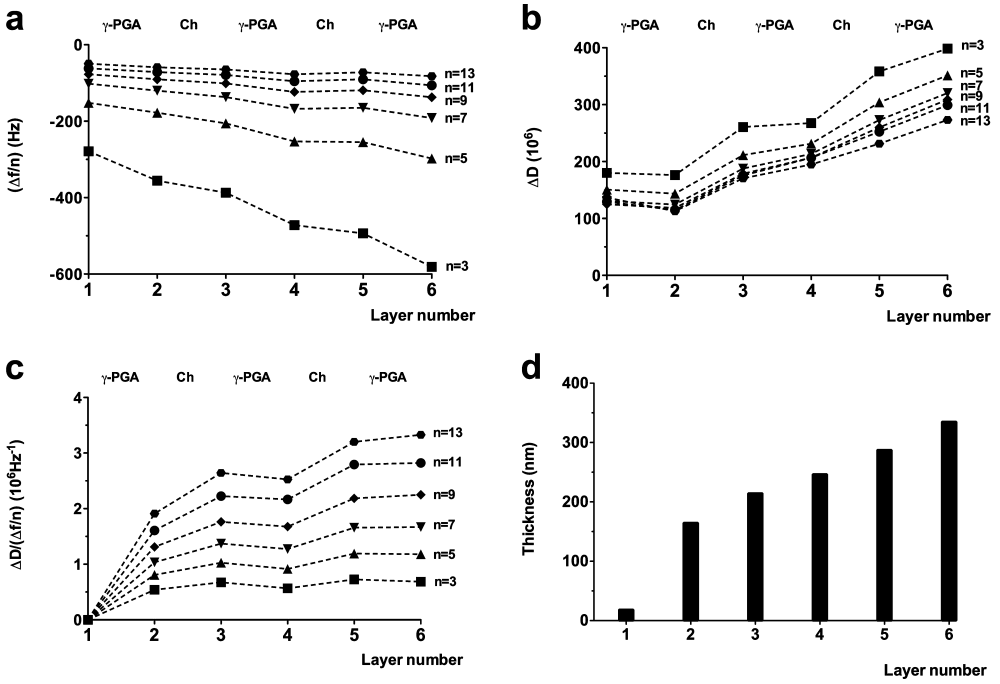

Figure 7. Normalized frequency, dissipation change, and dissipation energy per unit of mass added to the surface for the overtones n = 3, 5, 7, 9, 11, and 13 and Voigt-modeled thickness of the PEM films after each layer deposition. (a) Normalized change in frequency ($\Delta f/n$), (b) dissipation (ΔD) change, (c) $\Delta D/(\Delta f/n)$ ratio, and (d) evolution of the films' thickness. Layer 1: ellipsometric film thickness of the Ch spin-coated film (average of 18 ROIs, n = 2); layers 2–6: data estimated through the Voigt viscoelastic model (n = 3, 5, 7, 9, 11, and 13); ρFld = 1008 kg/m^3; ηFld = 0.001 Pa·s; and ρL1 = 1200 kg/m^3.

Table 2. Comparison between Thicknesses Evolution (nm/%), Obtained through the Ellipsometry and QCM-D (Thickness$_{ellipsometry}$ and Thickness$_{QCM-D}$, Respectively), Highlighting the Contribution of Each Layer to the Final Thickness; C−O Stretching Peak Increment Determined from the FTIR-IRRAS Spectra, after the First γ-PGA Deposition; and the ζ Potential Difference from the EKA Analysis, Resulting from Each Layer Addition to the Substrate

	thickness$_{ellipsometry}$ (nm/%)^{a,b}		C−O str peak increment (%T)	|Δζ potentiall (mV)	thickness$_{QCM-D}$ (nm/%)^{a,b}	
layer 1	17	27		38	18^c	5
layer 2	17 + 12 = 29	19		30	18 + 147 = 165	45
layer 3	29 + 3 = 32	6	0.2	21	165 + 49 = 214	15
layer 4	32 + 16 = 48	25	1.2	16	214 + 33 = 247	9
layer 5	48 + 5 = 53	7	0.3	13	247 + 41 = 288	14
layer 6	53 + 10 = 63	16	2.4	7	288 + 47 = 335	11

$^a L_{B/b} = L_{A/a} + L_{increment}$, where $L_{B/b}$ represents the thickness of a top layer, $L_{A/a}$ is the thickness of the previously deposited layer, and $L_{increment}$ is the thickness increment between both layers. Capitulated letters refer to the QCM-D thicknesses, and the other ones refer to ellipsometric thicknesses. $^b L_{B/b} - L_{A/a}/L_{FINAL/Final} \times 100$, aiming to determine how much, in %, each layer contributes to the final thickness. ^{c}Ch film deposited onto the quartz crystal, obtained by spin-coating.

bending and C−N stretching vibrations of secondary amides of Ch, together with conformational changes in the layered film. (iv) From the EKA analysis, it is evident that the |Δζ potentiall decreases with increasing layer number as the multilayer is built up.

In Vitro Cytotoxicity Assessment. The cytotoxicity of Ch/γ-PGA PEM films was evaluated according to ISO 10993-5 using a mouse embryonic fibroblast cell line (NIH3T3). The aim was to evaluate the cytotoxicity of the material itself and the possible contribution of toxic leachable products.

NIH3T3 cells were cultured in direct contact with Ch films, Ch/γ-PGA PEMs, and TCPS (Figure 8a,b) during 3 days. NIH3T3 metabolic activity cultured in direct contact with the materials and in the presence of materials extracts was compared with standard metabolic activity (TCPS). This is indicated in Figure 8c,d, where the metabolic activity is represented as a percentage with respect to that on TCPS (100%).

After 6 h of cell seeding, NIH3T3 cell morphology and distribution in different substrates (TCPS, Ch, and PEMs) were similar (Figure 8b). After 24 h, NIH3T3 cells start to present a spindle shape, characteristic of this fibroblast cell line, which is maintained through the time of culture (Figure 8b). Concerning metabolic activity, NIH3T3 culture in direct and indirect contact with the Ch films and PEM films revealed higher values than those observed with standard culture substrates (TCPS). In addition, no significant differences were observed between Ch and PEM ($p < 0.05$). Overall, the results indicate an increase in metabolic activity during the 3 days of in vitro cell culture, which demonstrates an absence of materials toxicity.

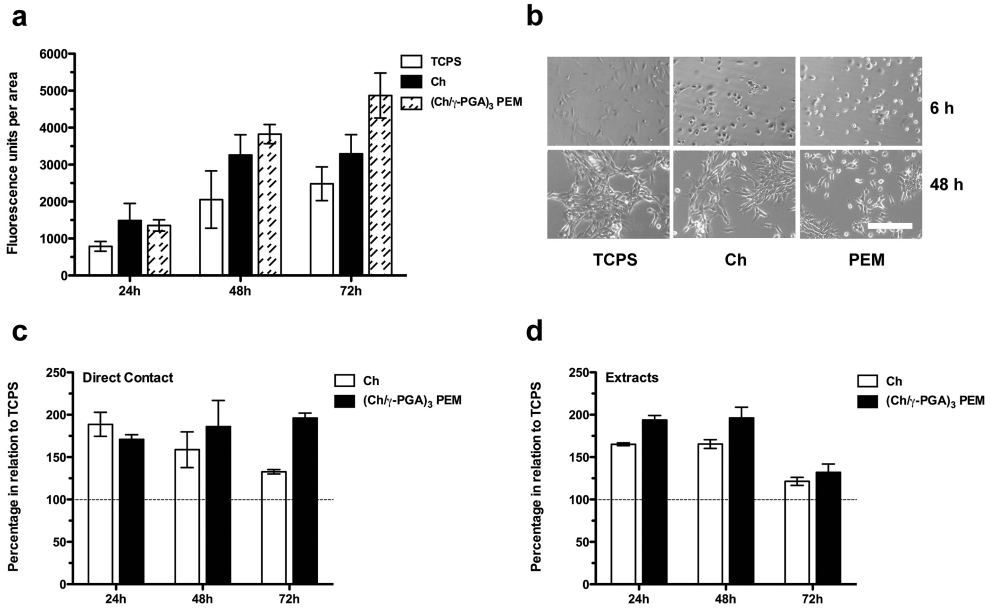

Figure 8. NIH3T3 metabolic activity of Ch and PEM films measured by Resazurin test. (a) Cells cultured directly onto the surface substrates. (b) Microscopy images taken to NIH3T3 cells adhered to TCPS discs, Ch, and $(Ch/\gamma\text{-}PGA)_3$ PEM films, after 6 and 48 h of cell seeding. Scale bar represents 200 μm, and it is applicable to all images. (c) Percentages of NIH3T3 metabolic activity, in relation to TCPS, of Ch and $(Ch/\gamma\text{- }PGA)_3$ PEM films, using NIH3T3 cultured directly onto the surface substrates, and (d) in the presence of extracts. Results are presented as mean ± SD (n = 3).

DISCUSSION

Multilayered films of Ch and γ-PGA were prepared by LbL self-assembly and analyzed through the combination of different techniques.

Imaging ellipsometry has demonstrated the multilayer buildup after each exposure to one of the polyelectrolyte solutions. However, as referred by Schlenoff and Dubas,[64] the term "layer" might be inadequate because considerable intermingling (interpenetration) of polymers may occur during adsorption. This fact was suggested by AFM imaging, in which heterogeneous surfaces were observed after deposition of six layers, both under dried and under hydrated conditions. The images show large structures, which relate to the so-called "islands", formed by complex coacervation of polyelectrolyte molecules. This was already reported for LbL films, such as in PEMs between poly(allylamine) hydrochloride (PAA) and poly(vinylsulfate) potassium salt (PVS),[65] poly(L-lysine) (PLL) and HA,[66] and Ch and HA.[67]

The electrostatic interaction between Ch and γ-PGA was confirmed by FTIR spectra. The appearance of the 1220 cm^{-1} peak suggests the presence of γ-PGA (Figure 4b,c), with a possible contribution of the in-phase combination of N−H in-plane bending and C−N stretching vibrations of secondary amides (trans form), present in both polymers (including the amide III of γ-PGA). Nevertheless, comparing the Ch and PEM spectra, a major contribution of γ-PGA to the peak height is suggested. Confirming the interaction between Ch and γ-PGA, peaks from C═O stretching and N−H bending bands increase with the layer number. This aspect is in accordance with other studies with Ch/γ-PGA hydrogels,[68] in which an increase in the peak intensity occurred with an increasing degree of complexation. The highest peak at 1100 cm^{-1} (Figure 4a) is a possibility when the polymer is produced microbially, as referred by Kunioka et al.[47] A step to remove polysaccharides was included in the γ-PGA purification method. Nevertheless, this small contamination may be identified in a FTIR spectrum. The shift in the position of the band located in the 1595−1716 cm^{-1} region to a lower wavenumber (Figure 4a) evokes conformational changes: a dipole rearrangement of the multilayers is suggested, with layer intermingling, a fact that relates to an increased electrostatic interaction between the polyions.[69] In the work of Boulmedais et al.,[70] spectrum shifts toward smaller wavenumbers were identified in the amide I band (1600−1700 cm^{-1}). This occurred after contact of the PEM film (layers of PGA and poly(allylamine)) with a PGA solution; the other polyion (poly(allylamine)) does not display characteristics vibration bands in this region of the spectrum, which facilitates spectrum analysis. In our work, the spectrum has a contribution of Ch in this region, and with increased polyion deposition, a shift of the band located in the 1595−1716 cm^{-1} with the increasing number of polyions layers deposition was observed. A shift of this band to a lower wavenumber has already been identified in Ch/γ-PGA hydrogels[40] and can be related with structural rearrangements of the γ-PGA molecular conformation to a β-sheet structure.[70−72]

Electrokinetic analysis was used for measuring surface electrical charge. From the negatively charged gold substrate (in accordance with previous studies[73,74]), ζ potential increases upon deposition of the first Ch layer and decreases with the subsequent γ-PGA deposition. As defended by Schlenoff et al.,[75] the surface electrical charge reversal allows steady-state increments of oppositely charged polyelectrolyte to the substrates surface, by sequential adsorption steps, which is a requirement for polyion multilayer assembly driven by electrostatic interactions.

Interestingly, a decrease in the amplitude of the ζ potential inversion was observed with the increase in layer number, which suggests polyelectrolyte adsorption on uncovered segments of the underlying layer and subsequent intermingling of the deposited layers.[73] The intense ζ potential inversion after

dx.doi.org/10.1021/bm2008235 | Biomacromolecules 2011, 12, 4183−4195

the first γ-PGA deposition suggests a higher amount of the anionic γ-PGA being adsorbed due to the first Ch layer, compensating for the presence of a larger number of protonated charges than in subsequent steps.

The electrical potentials recorded may be influenced by the presence of the gold substrate because the thin polymeric layered structures may not constitute an effective shield originated by the gold substrates. However, changes in the ζ potential are sufficiently large to conclude that electrostatic interactions were responsible for the LbL buildup.

To assess LbL buildup in real time, QCM-D was used to estimate the variation of frequency and dissipation values with the mass deposited in each layer. Each polyelectrolyte addition lead to a frequency decrease, implying that mass was being added onto the substrates surface. This agrees with current opinion on the process of self-assembly of LbL films.[60,76] Also, the PEM construction in these experiments was stable at the pH investigated and did not require the use of additional organic solvents, as it did in previous studies.[36,37]

The large frequency variation during contact of the surface with the polyanion solution, and the slightly smaller response with the polycation, is related to the fact that the first layer was deposited by spin-coating employing a Ch solution concentration (5 mg/mL) 25 times higher than the one used for the LbL deposition (0.2 mg/mL).

The ratio $\Delta D/(\Delta f/n)$ was determined from the QCM-D results (Figure 7c). This parameter was used to represent the aggregate viscoelasticity of an adsorbed layer: small and compact layers yield small $\Delta D/(\Delta f/n)$ values, whereas open structures or relatively thick layers yield larger values.[76] The higher increase in the $\Delta D/(\Delta f/n)$ ratio after the Ch layer deposition (an exception was the first γ-PGA addition) suggests that the γ-PGA are more compact than the Ch layers. It is hypothesized that the lower $\Delta D/(\Delta f/n)$ ratio for the γ-PGA layers relates to a decrease in the water content of the multilayer and to the probable stronger interaction between the polyelectrolytes. As a result, more compact layers would form, with a higher amount of adsorbed polymer, as more polyelectrolyte is needed for the surface charge overcompensation. The same tendency was previously described in the study of multilayers formed by the sodium salt of poly(4-styrenesulfonate), PSS, and triblock copolymers of the form PDMAEMA-PCL-PDMAEMA (PDMAEMA corresponding to poly[2-(*N*,*N*-dimethylamino)ethyl methacrylate) and PCL to poly(ε-caprolactone).[77]

In conjunction with the latter arguments, the lower water content accompanying the γ-PGA additions may also suggest that the polyanion has changed its conformation, becoming more flat and compact on the substrate, and with less trapped water than the adsorbed Ch layers. In the work of He et al.,[72] it has been reported that γ-PGA has a helical conformation in solution and may adopt a β-sheet conformation with increasing concentration, ionic strength, pH, and even complexation. In the preparation of the Ch/γ-PGA PEM films, a buffer solution with 0.05 M Tris-HCl and 0.15 M of NaCl was used between each layer deposition. Also, the γ-PGA was dissolved in the same buffer. Hence, when the polyanion was added to the surface, an increase in the systems entropy is likely to occur, leading the polyelectrolyte chains in solution to adopt a loopy conformation, which facilitates PEM formation with respect to a β-sheet conformation, with the subsequent decrease in the water content of the multilayer, as the assembly progresses.[2,78]

The Ch tertiary structure and its resultant layer on the surface likely imbibe a larger amount of trapped water than the γ-PGA layer, causing less rigidity on the PEM film and a higher dissipation energy.[76,79] Because Ch has a rigid and stereoregular structure containing bulky pyranose rings, the PEM formation can induce a conformational change of the other polyelectrolyte, if the latter has a nonrigid structure. It has been reported that a nonrigid structure is more prone to conformational changes.[21] Moreover, the γ-PGA solution has a lower G'' value than the Ch solution (Table 1). The substantial difference in the $\Delta D/(\Delta f/n)$ ratio values appear to be mainly due to polyelectrolyte adsorption and consequent formation of complex coacervates with the Ch, as it has also been established by the previous characterization methods.

Table 2 resumes increments of different parameters (from ellipsometry, FTIR, EKA and QCM-D analyses) with layer number. Comparing the distinct increments given by the different characterization methods, a heterogeneous distribution of the PEMs formed after each polyion deposition can be observed. The major influence of the first deposited layers in PEM formation is consistent, suggesting that the Ch deposition by spin-coating favors the electrostatic interaction with the subsequent layers. The greatest increment appears in layer 2 (γ-PGA deposition), as it is clear from all characterization methods. As LbL deposition proceeds, more charges become neutralized. EKA measurements stress this tendency, as indicated by the decrease in the amplitude of the ζ potential inversion. That is also highlighted by the ellipsometric data. The analyses in a dried state provide good cues on what is happening at the molecular level. However, changes are more realistically assessed in a wet state, namely, when the LbL PEMs are built in situ, using the QCM-D. As indicated in the Results section, analysis of the raw data analyzed with the help of the Voigt model, provides a more realistic approach to the viscoelastic properties of the multilayers.

Previous cytotoxicity studies involving Ch/γ-PGA PEC hydrogels were carried out using commercially available γ-PGA.[38−40] The complexed structures have been tested in direct contact with rat osteosarcoma (ROS) cells,[38] normal human dermal fibroblast (NHDF) cell line,[39] and 3T3 fibroblasts.[40] One crucial aspect to consider is that in this investigation γ-PGA with a high purity as used. This is particularly important because access to high-quality γ-PGA is not easy.[33]

With the γ-PGA microbially produced by our team, the tests performed directly onto the Ch/γ-PGA PEM films and in the presence of its leachable contents showed no cytotoxic effects toward the cells tested (fibroblasts).

CONCLUSIONS

This study describes the production of PEM films with Ch and γ-PGA, using LbL deposition through the dip-coating method. For the first time, an extensive characterization of Ch and γ-PGA electrostatic interaction was performed. For that, different techniques were combined. An increase in multilayer thickness and surface roughness with increasing layer number was observed via ellipsometry, QCM-D, and AFM; the chemical composition analysis (FTIR) revealed the presence of both Ch and γ-PGA in the self-assembled structures and highlighted the electrostatic interaction between the polyions; surface electrical charge reversal was also observed after each layer addition, which confirms the contribution of the charge compensation to the polyions assembly. Ch/γ-PGA PEMs cytotoxicity was also evaluated. Overall, this study demonstrates that Ch and γ-PGA

can easily form cytocompatible multilayered structures, rendering them suitable for various biomedical studies, including delivery of biologically active molecules and as 2D substrates for investigating cell−biomaterial interactions, namely, in applications related to tissue regeneration.

AUTHOR INFORMATION

Corresponding Author

*E-mail: joana.antunes@ineb.up.pt.

ACKNOWLEDGMENTS

This work was financed by FEDER funds through the *Programa Operacional Factores de Competitividade* − COMPETE, by Portuguese funds through FCT − *Fundação para a Ciência e a Tecnologia* in the framework of the project PEst-C/SAU/LA0002/2011 and by DISC Regeneration project, with the grant agreement no. NMP3-LA-2008-213904 (FP7). Joana Antunes is grateful to FCT for the Ph.D. grant SFRH/BD/48554/2008. We gratefully acknowledge several INEB members: Dr. Isabel F. Amaral, Dr. Mª Cristina L. Martins, Dr. Cristina C. Barrias, Dr. Cristina C. Ribeiro, the research technicians Manuela Brás and Ricardo V. Silva, for their contribution in the materials characterization, and Dr. Ana Paula Pêgo and Dr. Hugo Oliveira for providing the mouse embryonic fibroblast cell line (NIH3T3). We would like also to thank Dr. Ana Azevedo and Prof. Dr. João Costa Pessoa from Instituto Superior Técnico - Universidade Técnica de Lisboa for providing the access to Circular Dichroism technique and the help on results analysis; Eng. Renate Kohl from Anton Paar GmbH, Dr. Jürgen Schlütter from LOT-Oriel GmbH & Co. KG and Dr. Fredrik Andersson from Q-Sense for the technical support, for the help in the EKA and QCM-D analyses, and results discussion; and to the Laboratory for Scanning Probe Microscopy, at CEMUP, for their help in the AFM measurements.

REFERENCES

(1) Bertrand, P.; Jonas, A.; Laschewsky, A.; Legras, R. Ultrathin polymer coatings by complexation of polyelectrolytes at interfaces: suitable materials, structure and properties. *Macromol. Rapid Commun.* **2000**, *21*, 319−348.

(2) Schonhoff, M. Layered polyelectrolyte complexes: physics of formation and molecular properties. *J. Phys.: Condens. Matter* **2003**, *15*, R1781−R1808.

(3) von Klitzing, R. Internal structure of polyelectrolyte multilayer assemblies. *Phys. Chem. Chem. Phys.* **2006**, *8*, 5012−5033.

(4) Iler, R. K. Multilayers of colloidal particles. *J. Colloid Interface Sci.* **1966**, *21*, 569−594.

(5) Zhang, X.; Chen, H.; Zhang, H. Y. Layer-by-layer assembly: from conventional to unconventional methods. *Chem. Commun.* **2007**, *14*, 1395−1405.

(6) Decher, G.; Hong, J. D.; Schmitt, J. Buildup of ultrathin multilayer films by a self-assembly process. 3. Consecutively alternating adsorption of anionic and cationic polyelectrolytes on charged surfaces. *Thin Solid Films* **1992**, *210*, 831−835.

(7) Boudou, T.; Crouzier, T.; Ren, K. F.; Blin, G.; Picart, C. Multiple functionalities of polyelectrolyte multilayer films: new biomedical applications. *Adv. Mater.* **2010**, *22*, 441−467.

(8) Schlenoff, J. B. Retrospective on the future of polyelectrolyte multilayers. *Langmuir* **2009**, *25*, 14007−14010.

(9) Ariga, K.; Hill, J. P.; Ji, Q. M. Layer-by-layer assembly as a versatile bottom-up nanofabrication technique for exploratory research and realistic application. *Phys. Chem. Chem. Phys.* **2007**, *9*, 2319−2340.

(10) Meng, S.; Liu, Z.; Shen, L.; Guo, Z.; Chou, L. L.; Zhong, W.; Du, Q.; Ge, J. The effect of a layer-by-layer chitosan-heparin coating on the endothelialization and coagulation properties of a coronary stent system. *Biomaterials* **2009**, *30*, 2276−2283.

(11) De Geest, B. G.; Jonas, A. M.; Demeester, J.; De Smedt, S. C. Glucose-responsive polyelectrolyte capsules. *Langmuir* **2006**, *22*, 5070−5074.

(12) Dimitrova, M.; Affolter, C.; Meyer, F.; Nguyen, I.; Richard, D. G.; Schuster, C.; Bartenschlager, R.; Voegel, J.-C.; Ogier, J.; Baumert, T. F. Sustained delivery of siRNAs targeting viral infection by cell-degradable multilayered polyelectrolyte films. *Proc. Natl. Acad. Sci. U.S.A.* **2008**, *105*, 16320−16325.

(13) Crouzier, T.; Ren, K.; Nicolas, C.; Roy, C.; Picart, C. Layer-by-layer films as a biomimetic reservoir for rhBMP-2 delivery: controlled differentiation of myoblasts to osteoblasts. *Small* **2009**, *5*, 598−608.

(14) He, L. Z.; Dexter, A. F.; Middelberg, A. P. J. Biomolecular engineering at interfaces. *Chem. Eng. Sci.* **2006**, *61*, 989−1003.

(15) Chua, P. H.; Neoh, K. G.; Shi, Z.; Kang, E. T. Structural stability and bioapplicability assessment of hyaluronic acid-chitosan polyelectrolyte multilayers on titanium substrates. *J. Biomed. Mater. Res., Part A* **2008**, *87A*, 1061−1074.

(16) Decher, G. Fuzzy nanoassemblies: toward layered polymeric multicomposites. *Science* **1997**, *277*, 1232−1237.

(17) Ozin, G. A.; Hou, K.; Lotsch, B. V.; Cademartiri, L.; Puzzo, D. P.; Scotognella, F.; Ghadimi, A.; Thomson, J. Nanofabrication by self-assembly. *Mater. Today* **2009**, *12*, 12−23.

(18) Dubas, S. T.; Schlenoff, J. B. Factors controlling the growth of polyelectrolyte multilayers. *Macromolecules* **1999**, *32*, 8153−8160.

(19) Kumar, M.; Muzzarelli, R. A. A.; Muzzarelli, C.; Sashiwa, H.; Domb, A. J. Chitosan chemistry and pharmaceutical perspectives. *Chem. Rev.* **2004**, *104*, 6017−6084.

(20) Yi, H. M.; Wu, L. Q.; Bentley, W. E.; Ghodssi, R.; Rubloff, G. W.; Culver, J. N.; Payne, G. F. Biofabrication with chitosan. *Biomacromolecules* **2005**, *6*, 2881−2894.

(21) Berger, J.; Reist, M.; Mayer, J. M.; Felt, O.; Gurny, R. Structure and interactions in chitosan hydrogels formed by complexation or aggregation for biomedical applications. *Eur. J. Pharm. Biopharm.* **2004**, *57*, 35−52.

(22) Rinaudo, M. Chitin and chitosan: properties and applications. *Prog. Polym. Sci.* **2006**, *31*, 603−632.

(23) Sogias, I. A.; Khutoryanskiy, V. V.; Williams, A. C. Exploring the factors affecting the solubility of chitosan in water. *Macromol. Chem. Phys.* **2010**, *211*, 426−433.

(24) Sorlier, P.; Denuziere, A.; Viton, C.; Domard, A. Relation between the degree of acetylation and the electrostatic properties of chitin and chitosan. *Biomacromolecules* **2001**, *2*, 765−772.

(25) Krayukhina, M. A.; Samoilova, N. A.; Yamskov, I. A. Polyelectrolyte complexes of chitosan: formation, properties, and applications. *Usp. Khim.* **2008**, *77*, 854−869.

(26) Buescher, J. M.; Margaritis, A. Microbial biosynthesis of polyglutamic acid biopolymer and applications in the biopharmaceutical, biomedical and food industries. *Crit. Rev. Biotechnol.* **2007**, *27*, 1−19.

(27) Shih, I. L.; Van, Y. T.; Shen, M. H. Biomedical applications of chemically and microbiologically synthesized poly(glutamic acid) and poly(lysine). *Mini-Rev. Med. Chem.* **2004**, *4*, 179−188.

(28) Nelson, D. L.; Cox, M. M. Amino Acids, Peptides and Proteins. In *Lehninger Principles of Biochemistry*, 4th ed.; W. H. Freeman and Company: New York, 2005; pp 78−79.

(29) Edde, B.; Rossier, J.; Lecaer, J. P.; Desbruyeres, E.; Gros, F.; Denoulet, P. Posttranslational glutamylation of alpha-tubulin. *Science* **1990**, *247*, 83−85.

(30) Candela, T.; Fouet, A. Poly-γ-glutamate in bacteria. *Mol. Microbiol.* **2006**, *60*, 1091−1098.

(31) Rhie, G. E.; Roehrl, M. H.; Mourez, M.; Collier, R. J.; Mekalanos, J. J.; Wang, J. Y. A dually active anthrax vaccine that confers protection against both bacilli and toxins. *Proc. Natl. Acad. Sci. U.S.A.* **2003**, *100*, 10925−10930.

(32) Schneerson, R.; Kubler-Kielb, J.; Liu, T. Y.; Dai, Z. D.; Leppla, S. H.; Yergey, A.; Backlund, P.; Shiloach, J.; Majadly, F.; Robbins, J. B. Poly(γ-D-glutamic acid) protein conjugates induce IgG antibodies in

mice to the capsule of Bacillus anthracis: a potential addition to the anthrax vaccine. *Proc. Natl. Acad. Sci. U.S.A.* **2003**, *100*, 8945−8950.
(33) Prescott, A. G.; Stock, L. R., II. Method for Producing Medical and Commercial Grade Poly-γ-glutamic Acid of High Molecular Weight. U. S. Patent 20050095679, 2005.
(34) Prodhomme, E. J. F.; Tutt, A. L.; Glennie, M. J.; Bugg, T. D. H. Multivalent conjugates of poly-γ-D-glutamic acid from *Bacillus licheniformis* with antibody F(ab′) and glycopeptide ligands. *Bioconjugate Chem.* **2003**, *14*, 1148−1155.
(35) Sutherland, M. D.; Thorkildson, P.; Parks, S. D.; Kozel, T. R. In vivo fate and distribution of poly-γ-D-glutamic acid, the capsular antigen from *Bacillus anthracis*. *Infect. Immun.* **2008**, *76*, 899−906.
(36) Serizawa, T.; Goto, H.; Kishida, A.; Endo, T.; Akashi, M. Improved alternate deposition of biodegradable naturally occurring polymers onto a quartz crystal microbalance. *J. Polym. Sci., Part A: Polym. Chem.* **1999**, *37*, 801−804.
(37) Tachaboonyakiat, W.; Serizawa, T.; Endo, T.; Akashi, M. The influence of molecular weight over the ultrathin films of biodegradable polyion complexes between chitosan and poly(γ-glutamic acid). *Polym. J.* **2000**, *32*, 481−485.
(38) Hsieh, C. Y.; Tsai, S. P.; Wang, D. M.; Chang, Y. N.; Hsieh, H. J. Preparation of γ-PGA/chitosan composite tissue engineering matrices. *Biomaterials* **2005**, *26*, 5617−5623.
(39) Kang, H. S.; Park, S. H.; Lee, Y. G.; Son, T. I. Polyelectrolyte complex hydrogel composed of chitosan and poly(γ-glutamic acid) for biological application: preparation, physical properties, and cytocompatibility. *J. Appl. Polym. Sci.* **2007**, *103*, 386−394.
(40) Tsao, C. T.; Chang, C. H.; Lin, Y. Y.; Wu, M. F.; Wang, J. L.; Han, J. L.; Hsieh, K. H. Antibacterial activity and biocompatibility of a chitosan-γ-poly(glutamic acid) polyelectrolyte complex hydrogel. *Carbohydr. Res.* **2010**, *345*, 1774−1780.
(41) Hajdu, I.; Bodnar, M.; Filipcsei, G.; Hartmann, J. F.; Daroczi, L.; Zrinyi, M.; Borbely, J. Nanoparticles prepared by self-assembly of chitosan and poly-γ-glutamic acid. *Colloid Polym. Sci.* **2008**, *286*, 343−350.
(42) Lin, Y. H.; Chung, C. K.; Chen, C. T.; Liang, H. F.; Chen, S. C.; Sung, H. W. Preparation of nanoparticles composed of chitosan/poly-γ-glutamic acid and evaluation of their permeability through Caco-2 cells. *Biomacromolecules* **2005**, *6*, 1104−1112.
(43) Imoto, T.; Kida, T.; Matsusaki, M.; Akashi, M. Preparation and unique pH-responsive properties of novel biodegradable nanocapsules composed of poly(γ-glutamic acid) and chitosan as weak polyelectrolytes. *Macromol. Biosci.* **2010**, *10*, 271−277.
(44) Crompton, K. E.; Goud, J. D.; Bellamkonda, R. V.; Gengenbach, T. R.; Finkelstein, D. I.; Horne, M. K.; Forsythe, J. S. Polylysine-functionalised thermoresponsive chitosan hydrogel for neural tissue engineering. *Biomaterials* **2007**, *28*, 441−449.
(45) Brugnerotto, J.; Lizardi, J.; Goycoolea, F. M.; Arguelles-Monal, W.; Desbrieres, J.; Rinaudo, M. An infrared investigation in relation with chitin and chitosan characterization. *Polymer* **2001**, *42*, 3569−3580.
(46) Terbojevich, M.; Cosani, A.; Muzzarelli, R. A. A. Molecular parameters of chitosans depolymerized with the aid of papain. *Carbohydr. Polym.* **1996**, *29*, 63−68.
(47) Kunioka, M.; Goto, A. Biosynthesis of poly(γ-glutamic acid) from L-glutamic acid, citric-acid, and ammonium-sulfate in *Bacillus subtilis* IFO3335. *Appl. Microbiol. Biotechnol.* **1994**, *40*, 867−872.
(48) Kubota, H.; Matsunobu, T.; Uotani, K.; Takebe, H.; Satoh, A.; Tanaka, T.; Taniguchi, M. Production of poly(γ-glutamic acid) by *Bacillus subtilis* F-2-01. *Biosci., Biotechnol., Biochem.* **1993**, *57*, 1212−1213.
(49) Ashiuchi, M.; Soda, K.; Misono, H. A poly-γ-glutamate synthetic system of Bacillus subtilis IFO 3336: gene cloning and biochemical analysis of poly-γ-glutamate produced by *Escherichia coli* clone cells. *Biochem. Biophys. Res. Commun.* **1999**, *263*, 6−12.
(50) Yamaguchi, F.; Ogawa, Y.; Kikuchi, M.; Yuasa, K.; Motai, H. Detection of γ-polyglutamic acid (γ-PGA) by SDS-PAGE. *Biosci., Biotechnol., Biochem.* **1996**, *60*, 255−258.
(51) Scolnik, Y.; Portnaya, I.; Cogan, U.; Tal, S.; Haimovitz, R.; Fridkin, M.; Elitzur, A. C.; Deamer, D. W.; Shinitzky, M. Subtle differences in structural transitions between poly-L- and poly-D-amino acids of equal length in water. *Phys. Chem. Chem. Phys.* **2006**, *8*, 333−339.
(52) Martins, M. C. L.; Ratner, B. D.; Barbosa, M. A. Protein adsorption on mixtures of hydroxyl- and methylterminated alkanethiols self-assembled monolavers. *J. Biomed. Mater. Res., Part A* **2003**, *67A*, 158−171.
(53) Gehanno, V.; Freitas, P. P.; Veloso, A.; Ferreira, J.; Almeida, B.; Sousa, J. B.; Kling, A.; Soares, J. C.; da Silva, M. F. Ion beam deposition of Mn-Ir spin valves. *IEEE Trans. Magn.* **1999**, *35*, 4361−4367.
(54) Ambrosio, L.; Borzacchiello, A.; Netti, P. A.; Nicolais, L. Rheological study on hyaluronic acid and its derivative solutions. *J. Macromol. Sci., Part A: Pure Appl.Chem.* **1999**, *A36*, 991−1000.
(55) Horcas, I.; Fernandez, R.; Gomez-Rodriguez, J. M.; Colchero, J.; Gomez-Herrero, J.; Baro, A. M. WSXM: A software for scanning probe microscopy and a tool for nanotechnology. *Rev. Sci. Instrum.* **2007**, *78*, 1.
(56) Martins, M. C. L.; Ochoa-Mendes, V.; Ferreira, G.; Barbosa, J. N.; Curtin, S. A.; Ratner, B. D.; Barbosa, M. A. Interactions of leukocytes and platelets with poly(lysine/leucine) immobilized on tetraethylene glycol-terminated self-assembled monolayers. *Acta Biomater.* **2011**, *7*, 1949−1955.
(57) Werner, C.; Konig, U.; Augsburg, A.; Arnhold, C.; Korber, H.; Zimmermann, R.; Jacobasch, H. J. Electrokinetic surface characterization of biomedical polymers - a survey. *Colloids Surf., A* **1999**, *159*, 519−529.
(58) Fairbrother, F.; Mastin, H. Studies in electro-endosmosis part I. *J. Chem. Soc.* **1924**, *125*, 2319−2330.
(59) Voinova, M. V.; Rodahl, M.; Jonson, M.; Kasemo, B. Viscoelastic acoustic response of layered polymer films at fluid-solid interfaces: continuum mechanics approach. *Phy. Scr.* **1999**, *59*, 391−396.
(60) Hook, F.; Kasemo, B.; Nylander, T.; Fant, C.; Sott, K.; Elwing, H. Variations in coupled water, viscoelastic properties, and film thickness of a Mefp-1 protein film during adsorption and cross-linking: a quartz crystal microbalance with dissipation monitoring, ellipsometry, and surface plasmon resonance study. *Anal. Chem.* **2001**, *73*, 5796−5804.
(61) Hook, F.; Rodahl, M.; Brzezinski, P.; Kasemo, B. Measurements using the quartz crystal microbalance technique of ferritin monolayers on methyl-thiolated gold: dependence of energy dissipation and saturation coverage on salt concentration. *J. Colloid Interface Sci.* **1998**, *208*, 63−67.
(62) Larsson, C.; Rodahl, M.; Hook, F. Characterization of DNA immobilization and subsequent hybridization on a 2D arrangement of streptavidin on a biotin-modified lipid bilayer supported on SiO_2. *Anal. Chem.* **2003**, *75*, 5080−5087.
(63) Sauerbrey, G. Verwendung von schwingquarzen zur wagung dunner schichten und zur mikrowagung. *Z. Phys.* **1959**, *155*, 206−222.
(64) Schlenoff, J. B.; Dubas, S. T. Mechanism of polyelectrolyte multilayer growth: charge overcompensation and distribution. *Macromolecules* **2001**, *34*, 592−598.
(65) Kim, D. K.; Han, S. W.; Kim, C. H.; Hong, J. D.; Kim, K. Morphology of multilayers assembled by electrostatic attraction of oppositely charged model polyelectrolytes. *Thin Solid Films* **1999**, *350*, 153−160.
(66) Picart, C.; Lavalle, P.; Hubert, P.; Cuisinier, F. J. G.; Decher, G.; Schaaf, P.; Voegel, J. C. Buildup mechanism for poly(L-lysine)/hyaluronic acid films onto a solid surface. *Langmuir* **2001**, *17*, 7414−7424.
(67) Richert, L.; Lavalle, P.; Payan, E.; Shu, X. Z.; Prestwich, G. D.; Stoltz, J. F.; Schaaf, P.; Voegel, J. C.; Picart, C. Layer by layer buildup of polysaccharide films: physical chemistry and cellular adhesion aspects. *Langmuir* **2004**, *20*, 448−458.
(68) Tsao, C. T.; Hang, C. H.; Lin, Y. Y.; Wu, M. F.; Wang, J. L.; Young, T. H.; Han, J. L.; Hsieh, K. H. Evaluation of chitosan/γ-

poly(glutamic acid) polyelectrolyte complex for wound dressing materials. *Carbohydr. Polym.* **2011**, *84*, 812−819.
(69) Bonazzola, C.; Calvo, E. J. A Fourier transform infrared reflection-absorption spectroscopy study of redox polyelectrolyte films. *Langmuir* **2003**, *19*, 5279−5286.
(70) Boulmedais, F.; Ball, V.; Schwinte, P.; Frisch, B.; Schaaf, P.; Voegel, J. C. Buildup of exponentially growing multilayer polypeptide films with internal secondary structure. *Langmuir* **2003**, *19*, 440−445.
(71) Boulmedais, F.; Bozonnet, M.; Schwinte, P.; Voegel, J. C.; Schaaf, P. Multilayered polypeptide films: secondary structures and effect of various stresses. *Langmuir* **2003**, *19*, 9873−9882.
(72) He, L. M.; Neu, M. P.; Vanderberg, L. A. *Bacillus lichenformis* γ-glutamyl exopolymer: physicochemical characterization and U(VI) interaction. *Environ. Sci. Technol.* **2000**, *34*, 1694−1701.
(73) Chan, Y. H. M.; Schweiss, R.; Werner, C.; Grunze, M. Electrokinetic characterization of oligo- and poly(ethylene glycol)-terminated self-assembled monolayers on gold and glass surfaces. *Langmuir* **2003**, *19*, 7380−7385.
(74) Giesbers, M.; Kleijn, J. M.; Stuart, M. A. C. The electrical double layer on gold probed by electrokinetic and surface force measurements. *J. Colloid Interface Sci.* **2002**, *248*, 88−95.
(75) Schlenoff, J. B.; Ly, H.; Li, M. Charge and mass balance in polyelectrolyte multilayers. *J. Am. Chem. Soc.* **1998**, *120*, 7626−7634.
(76) Rodahl, M.; Hook, F.; Fredriksson, C.; Keller, C. A.; Krozer, A.; Brzezinski, P.; Voinova, M.; Kasemo, B. Simultaneous frequency and dissipation factor QCM measurements of biomolecular adsorption and cell adhesion. *Faraday Discuss.* **1997**, *107*, 229−246.
(77) Guzman, E.; San Miguel, V.; Peinado, C.; Ortega, F.; Rubio, R. C. Polyelectrolyte multilayers containing triblock copolymers of different charge ratio. *Langmuir* **2010**, *26*, 11494−11502.
(78) Salomaki, M.; Laiho, T.; Kankare, J. Counteranion-controlled properties of polyelectrolyte multilayers. *Macromolecules* **2004**, *37*, 9585−9590.
(79) Dutta, A. K.; Nayak, A.; Belfort, G. Viscoelastic properties of adsorbed and cross-linked polypeptide and protein layers at a solid-liquid interface. *J. Colloid Interface Sci.* **2008**, *324*, 55−60.